Journal of Alloys and Compounds 509 (2011) 3430–3434

Contents lists available at ScienceDirect

Journal of Alloys and Compounds

journal homepage: www.elsevier.com/locate/jallcom

Ultrasound-assisted preparation of titania–alumina support with high surface area and large pore diameter by modified precipitation method

Weiyang Wang[a], Yunquan Yang[a,*], Hean Luo[a], Tao Hu[a], Feng Wang[a,b], Wenying Liu[a]

[a] School of Chemical Engineering, Xiangtan University, Xiangtan City, Hunan 411105, PR China
[b] Department of Chemical and Environment Engineering, Hunan City University, Yiyang, 413000, PR China

ARTICLE INFO

Article history:
Received 26 September 2010
Received in revised form
12 December 2010
Accepted 15 December 2010
Available online 22 December 2010

Keywords:
Ultrasound
Precipitation
Composite materials
Titania–alumina
Surface area

ABSTRACT

Titania–alumina supports were prepared successfully using the ultrasound-assisted precipitation method. The resulting supports were characterized by fourier transform infrared analysis (FTIR), scanning electron microscope (SEM), X-ray diffraction (XRD) and N_2 physisorption. The effects of precipitants, washing method and the addition of surfactant CTAB were studied. The supports prepared with NH_4HCO_3 showed better textural properties compared with that with $NH_3{\cdot}H_2O$, which was attributed to the low NH_4^+ release rate of NH_4HCO_3. TiO_2–Al_2O_3 support with S_{BET} = 283 m^2/g, V_p = 2.34 mL/g and D_p = 33.0 nm was obtained with this modified precipitation method.

1. Introduction

It is well known that the chemical and structural characteristics of the support are very important as well as the nature and the structure of the active phase in the supported catalysts. TiO_2, being a good support candidate or catalyst, was applied into many catalysis fields such as reduction [1], oxidation [2,3], hydrogenation [4,5] and photocatalytic [6,7], but they have no pore system and the relatively low specific surface area, limiting their extensive application in catalysis. Normal alumina has a relative large specific surface area (200 m^2/g), but it still cannot meet the demand of chemical and petrochemical industry. The catalyst with a small pore diameter or a low specific surface area would decrease its catalytic activity by restricting the access of reactants to the catalytic sites or decreasing the numbers of activity sites per unit area. Rana et al. [8,9] studied the effects of the catalyst textural properties on the hydrotreating of heavy Maya crude oil. They found that the hydrodemetallization and hydrodearomatization activities mostly depend on the catalyst pore size distribution and the high hydrodesulfurization activity was attributed to the high metal dispersion and the high surface area of the supported catalysts. Thus, it is significant to consider the special surface area and the pore size of the support as important parameters for the supported catalyst to minimize the mass transfer influence and put the active sites to maximum dispersion.

Usually, the conventional precipitation process is carried out into the aqueous solution. The precipitates tend to aggregate and cannot be dispersed sufficiently because the nanoparticles need to decrease their high surface energy, leading to the serious agglomeration of nanoparticles and the bad textural properties of materials. Ultrasound can create a special reaction environment to deagglomerate nanoparticles and improve the reaction greatly owing to the strong chemical and mechanical effects of acoustic cavitation. For example, Palani et al. [10] adopted the sonochemical method to prepare the mesoporous silica SBA-15. They found that synthesis route effectively could reduce the total synthesis time from days to a few hours and the resultant materials exhibited a hexagonally ordered mesostructure with high surface area over 560 m^2/g, pore volume over 0.6 mL/g and large pore diameter in the range of 4.1–4.9 nm. The sonochemical processing has been developed to be a useful technique for the nanomaterial preparation [11–17]. Many nanomaterials such as TiO_2 [18,19], WO_3 [20], MoS_2 [21], Fe_2O_3 [22,23] and Al_2O_3 [24] have been prepared using this process.

In order to obtain the support with high surface area and large pore diameter, many other technologies were also used in the support preparation. For example, Vargas et al. [25] adopted the freeze–drying technique to eliminate water before the Al_2O_3–TiO_2 (20 wt% TiO_2) support drying and obtained the mesoporous support with a narrow single model pore size distribution (the most probable pore size 3.5 nm) and a high specific surface area

* Corresponding author.
E-mail address: yangyunquan@xtu.edu.cn (Y. Yang).

0925-8388/$ – see front matter.
doi:10.1016/j.jallcom.2010.12.119

(S_{BET} = 308 m^2/g). This technology could avoid the negative effects of water in the drying and maintained the original structure of support. In addition, surfactant such as hexadecyl trimethyl ammonium bromide (CTAB) or P123 was added to the as-prepared support during the preparation process, which could also obtain the support with high surface area and large pore size [26–30]. The conventional methods for the preparation of titania–alumina were mainly focused on co-precipitation method [31,32] and sol–gel method [33,34]. The former method used the available inorganic precursors as the starting materials and the cost was cheap while the latter method could obtain the material with a high surface area. Padmaja et al. [35] used the sol–gel method to prepare the titania–alumina mixed oxide and obtained the titania–alumina (the molar ratio 1:1) mixed oxide with S_{BET} = 200 m^2/g, V_p = 0.27 mL/g and D_p = 5.3 nm after calcined at 873 K. In this study, a new modified precipitation method was developed. Titania–alumina support with high specific surface area and large pore diameter was prepared with this new method.

2. Experimental

2.1. Synthesis of TiO_2–Al_2O_3 supports

The detailed preparation of TiO_2–Al_2O_3 (Ti/Al mole ratio = 1:2) support was described as follows. 13.35 g $AlCl_3$ and 9.5 g $TiCl_4$ were dissolved in a 500 mL water with pH 1. The precipitant solution such as $NH_3{\cdot}H_2O$ solution (A, 2.2 wt%) or NH_4HCO_3 solution (C, 10 wt%) was added to the above mixed solution to adjusted pH to 8 with vigorous agitation. This process was carried out in a commercial ultrasonic cleaning bath (from Kunshan Ultrasonic Instruments Co., China, model KQ2200DE, 40 kHz, 100 W) at 313 K for about 4 h. After the reaction completed, the white precipitate was collected and washed with water until no chloride ions could be detected with $AgNO_3$ solution in the filtrate and aged at 363 K for 1.0 h with water bath method. Then, the white precipitate was washed with anhydrous ethanol to remove water. The precipitate, CTAB and proper amount of anhydrous ethanol were mixed sufficiently and dried at 393 K in an oven for 12 h and finally calcined in a muffle oven at 873 K for 5 h. The resulting sample was denoted as D–M–L–Q where D stood for ultrasonic condition (U) or normal condition (N), M for the precipitants, L for water or ethanol, and Q for CTAB. The as-prepared support without adding CTAB was also prepared and denoted as D–M–N.

2.2. Characterization methods

Fourier transform infrared spectroscopy (FT-IR) characterization of the samples mixed with spectroscopy grade KBr was recorded on a NICOLET 380 FT-IR at room temperature, in the range of 4000–400 cm^{-1}. Nitrogen adsorption measurements were performed using Quantachrome's NOVA-2100e Surface Area instrument at 77 K with ultra high purity nitrogen gas. All samples were degassed under vacuum at 473 K for 10 h prior to measurement. The surface area was calculated by the BET (Brunauer–Emmett–Teller) equation and the pore size was determined by the BJH (Barret–Joyner–Hallender) model. Morphology and particle size were obtained by scanning electron microscopy (SEM) on a JEOL JSM-6360 electron microscopy. X-ray diffraction (XRD) tests were carried on a D/max2550 18 kW Rotating anode X-Ray Diffractometer Equipment with Cu Kα (λ = 1.5418 Å) radiation (40 kV, 300 mA).

3. Results and discussion

3.1. FTIR studies

Fig. 1 shows the FTIR spectra of CTAB, as-prepared supports and calcined supports. The bands around 3500 cm^{-1} and 1640 cm^{-1} were attributed to the stretching vibration and the bending vibration of adsorbed water. The bands around 960 cm^{-1}, 1487 cm^{-1}, 2853 cm^{-1} and 2923 cm^{-1} were corresponded to CTAB [28]. After the calcination, all of the bands of CTAB disappeared, suggesting that the surfactant was removed completely and there was not any CTAB in the calcined supports. However, the bands around 3400 cm^{-1} and 1640 cm^{-1} ascribed to water still appeared in the FTIR spectra of U–C–E–C sample, which was resulted from the adsorption of water vapor from the atmosphere due to the high surface area of the prepared support [36]. The broad overlapping peaks in the lower frequency range (450–800 cm^{-1}) were attributed to the Al–O (500–750 cm^{-1} [37,38]) and the anatase phase Ti–O (465 cm^{-1} [29,39]) infrared vibrations. Besides, compared with the FTIR spectra of the as-synthesized supports, the band of calcined supports at 1415 cm^{-1} decreased obviously, which was assigned to the formation of crystalline nanoparticles [40].

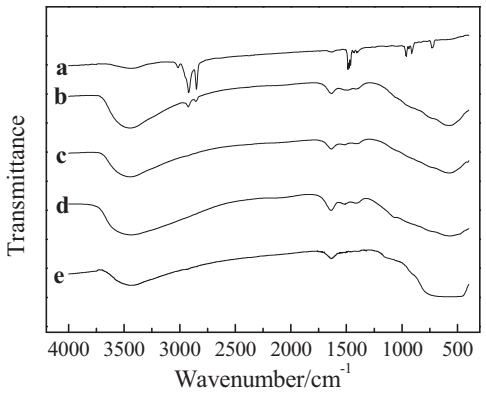

Fig. 1. FTIR spectra of (a) CTAB, (b) U–C–E–C(F), (c) U–C–E(F), (d) U–C–W(F) and (e) U–C–E–C samples (F represents the corresponding samples before calcination).

3.2. Morphology studies

The morphologies of TiO_2–Al_2O_3 supports prepared under different conditions are shown in Fig. 2. Obviously, the SEM images of the supports prepared with $NH_3{\cdot}H_2O$ under the normal condition showed more serious agglomeration than that with NH_4HCO_3 under the ultrasound condition. The main reasons could be explained as follows. On the one hand, in the ultrasound environment, the cavitation bubbles generated during the rarefaction or the negative pressure resulted in the strong chemical and mechanical effects. The chemical effects caused an environment with extremely high temperature of 5000 K and pressures of 50 atm, which could supply the required energy for the formation of microstructure and then decreased the surface free energy and improved the production rate of nucleation obviously. The pulverization of mechanical effects such as microjet effect could make the precipitates dispersed immediately. On the other hand, the NH_4^+ release rate of $NH_3{\cdot}H_2O$ solution was quicker than that of NH_4HCO_3 solution when the precipitant solutions had the same concentration. Correspondingly, the precipitation rate of NH_4HCO_3 was slower than that of $NH_3{\cdot}H_2O$ with the same dropping speed. The precipitates could be dispersed immediately and completely under the condition of ultrasound due to its strong chemical and mechanical effects. Hence, agglomeration phenomenon was inhibited effectively, which was beneficial to increase the specific surface area of support.

3.3. XRD studies

The XRD patterns of TiO_2–Al_2O_3 samples prepared with different precipitants are shown in Fig. 3. The peaks at 2θ = 38°, 46° and 67° were attributed to the (3 1 1), (4 0 0) and (4 4 0) reflections of γ–Al_2O_3 plane [40], respectively, which indicated that Al_2O_3 in the prepared TiO_2–Al_2O_3 support was in the form of active phase. The peaks at 2θ = 25°, 38°, 46°, 55°, 63°and 76° appeared in the XRD patterns was corresponded to the (1 0 1), (0 0 4), (2 0 0), (2 1 1), (2 0 4) and (2 1 5) reflections of the typical anatase TiO_2 plane [36]. The anatase phase, an activity phase in catalytic reactions, usually transformed to rutile phase at 773–873 K [41,42]. But not any peak could be attributed to the rutile phase TiO_2 in the XRD patterns of TiO_2–Al_2O_3 samples, indicating that TiO_2–Al_2O_3 support could keep TiO_2 in the anatase structure after the calcination at 873 K for 5 h. Because the homogenous dispersion of Al_2O_3 and

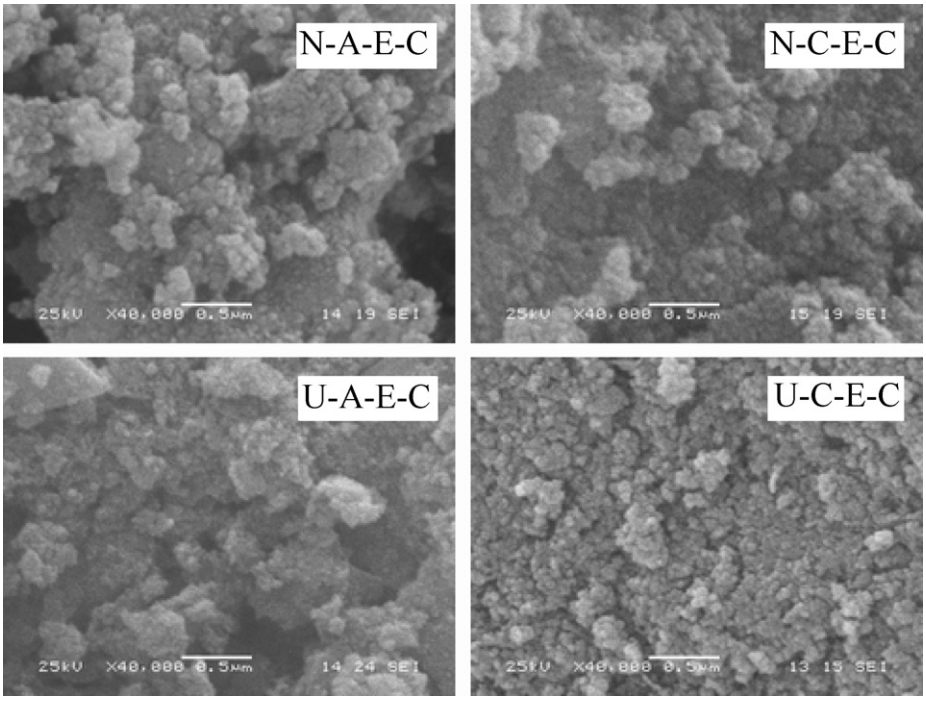

Fig. 2. . SEM images of N–A–E–C, N–C–E–C, U–A–E–C and U–C–E–C.

TiO_2 under the ultrasound condition could significantly prevent the aggregation of TiO_2 or Al_2O_3 nanoparticles, the stability of anatase TiO_2 could be improved, which could wide its application in the catalysis.

3.4. Nitrogen sorption studies

Generally, adsorption on mesoporous materials proceeds via multilayer adsorption followed by capillary condensation [43]. The adsorption process is initially similar to that on macroporous materials but at high pressures the adsorption amount rises very steeply due to capillary condensation in mesopores. The nitrogen adsorption–desorption isotherms measured for TiO_2–Al_2O_3 samples are shown in Fig. 4. The adsorption amount of each sample increased gradually as the relative pressure increased and then increased rapidly at high relative pressure ($P/P_0 > 0.7$), displaying a type II isotherm with H2 hysteresis loop. According to the nitrogen adsorption–desorption isotherms, it could be easy to see that the total adsorption of the sample prepared under the ultrasound condition was larger than that of the sample prepared under the normal condition and each sample showed a characteristic of mesoporous structure [44].

As shown in Table 1, the textural properties of TiO_2–Al_2O_3 supports were related to the precipitants, the washing method and the addition of surfactant. Both the pore volume and the average pore diameter of TiO_2–Al_2O_3 support precipitated with NH_4HCO_3 were bigger than that of with $NH_3{\cdot}H_2O$. For example, the average pore diameter of U–C–E–C was 33 nm, but the average pore diameter of U–A–E–C was only 18.8 nm. For the effect of washing method, the as-prepared supports, washed with anhydrous ethanol before drying, had higher specific surface area, larger pore volume and bigger pore diameter than that of without removing water before drying. When water in the as-prepared supports was replaced by anhydrous ethanol, the polar-OH was substituted by the nonpolar-OC_2H_5, which could be beneficial to inhibit the bridge between particles and increase the resistance capability of the shrinkage during drying, and then leaded to the increase of the surface area and the pore volume. When the as-prepared supports were not washed with anhydrous ethanol, the effects of different precipitants on the textural properties of supports were not

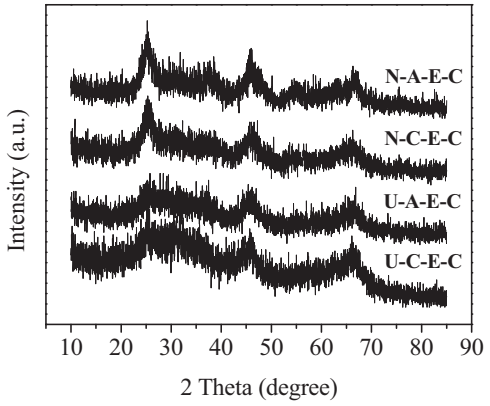

Fig. 3. XRD patterns of N–A–E–C, N–C–E–C, U–A–E–C and U–C–E–C.

Table 1
The textural properties of TiO_2–Al_2O_3 supports.

Samples	Specific surface area (S_{BET}, m^2/g)	Pore volume (V_p, mL/g)	Average pore diameter[a] (D_p, nm)
N–A–W	189	0.41	8.8
U–A–W	209	0.70	13.4
N–C–W	170	0.43	10.3
U–C–W	227	0.78	13.7
N–A–E	237	0.93	15.7
U–A–E	291	1.23	16.9
N–C–E	238	1.31	22.0
U–C–E	256	2.04	31.8
N–A–E–C	280	1.22	17.4
U–A–E–C	296	1.39	18.8
N–C–E–C	282	1.70	24.2
U–C–E–C	283	2.34	33.0

[a] The average pore diameters of the supports were calculated by the formula of $d = 4V_p/S_{BET}$.

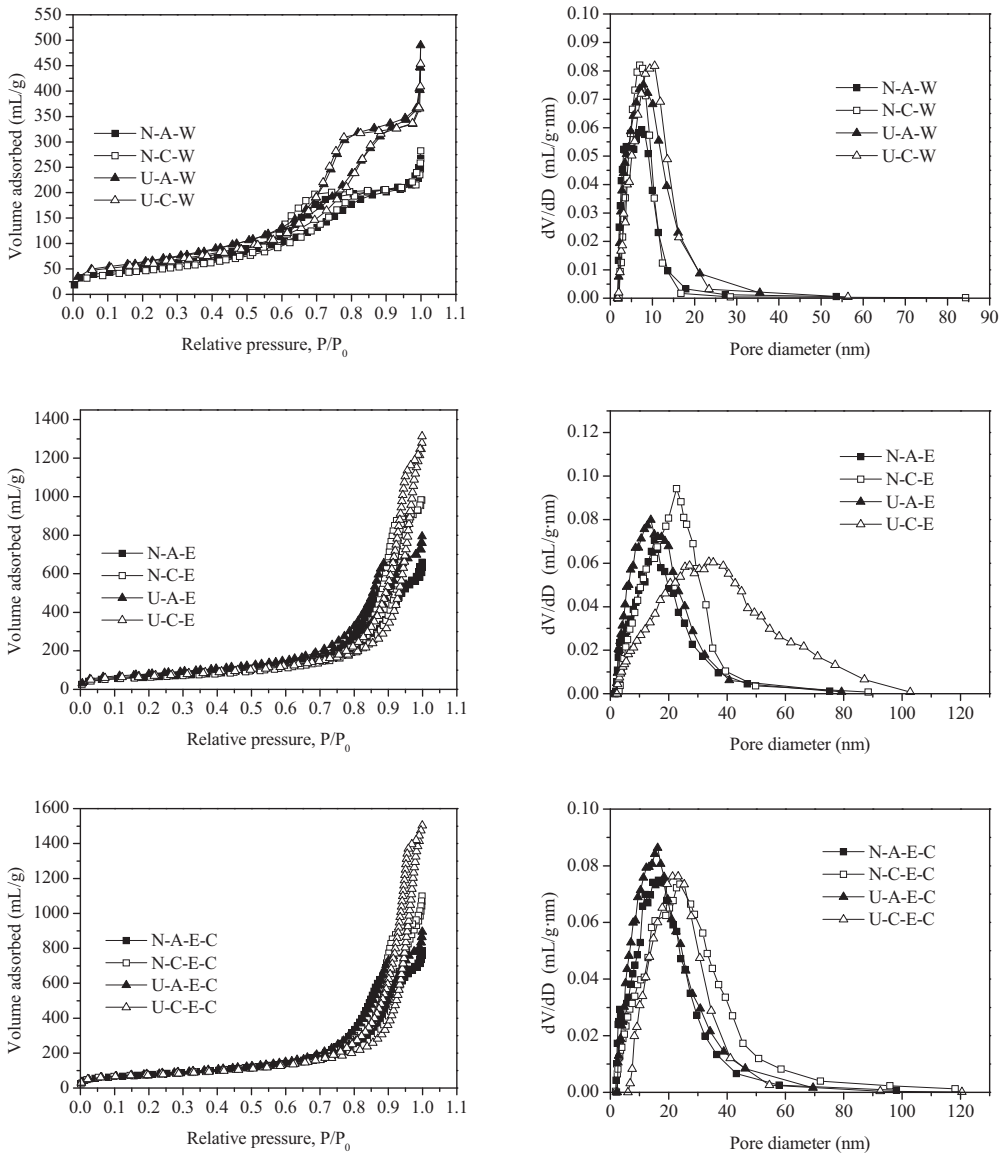

Fig. 4. Nitrogen adsorption–desorption isotherms and pore size distribution of TiO_2–Al_2O_3 supports.

very remarkable because of the significantly negative effects of water. The as-prepared precipitate, anhydrous ethanol and CTAB were stirred homogeneously under the condition of ultrasonic, the anhydrous ethanol could be removed from the as-prepared precipitate after drying at 393 K for 24 h, but CTAB was remained in the precipitate. The CTAB was incorporated in the as-prepared precipitate and played as a template, which had an inhibition effect for the formation of hydrogen bonding and some steric hindrance effect [45]. Therefore, CTAB could also prevent the decreases of pore diameter and pore volume in drying and calcination. Grzechowiak et al. [31] adopted coprecipitation method to obtain TiO_2–Al_2O_3 support (TiO_2 content 40 wt%) with the pore volume 0.80 mL/g and the average pore diameter 4.0 nm. Obviously, the textural properties of TiO_2–Al_2O_3 support prepared with the modified precipitation method were much better than that reported in the literatures.

4. Conclusions

A new method for the preparation of support with high surface area and large pore diameter was developed. Ultrasound could produce the strong chemical and mechanical effects, which was beneficial to inhibit the agglomeration of as-prepared nanoparticles. Using anhydrous ethanol to replace the water in the as-prepared support could hinder the particles agglomeration and then increased the specific surface area and the pore diameter significantly. Adding CTAB in the as-prepared support before calcination could enlarge the pore volume greatly. TiO_2–Al_2O_3 support with S_{BET} = 283 m^2/g, V_p = 2.34 mL/g and D_p = 33.0 nm was obtained using this method. The support with high specific surface area and big pore volume would be beneficial to the high dispersion of active metal and minimize the mass transfer influence. This modified precipitation method was also suitable for the preparation of other supports such as TiO_2, Al_2O_3, ZrO_2 and ZrO_2–Al_2O_3 with high surface area and large pore diameter.

Acknowledgements

This research was supported by Scientific Research Fund of Hunan Provincial Education Department (10K062) and Hunan Provincial Innovation Foundation for Postgraduate (CX2009B135).

References

[1] Y.J. Kim, H.J. Kwon, I. Nam, J.W. Choung, J.K. Kil, H.J. Kim, M.S. Cha, G.K. Yeo, Catal. Today 151 (2010) 244–250.
[2] G. Lu, X. Li, Z. Qu, Q. Zhao, H. Li, Y. Shen, G. Chen, Chem. Eng. J. 159 (2010) 242–246.
[3] Y. Azizi, V. Pitchon, C. Petit, Appl. Catal. A: Gen. 385 (2010) 170–177.
[4] A. Vicente, T. Ekou, G. Lafaye, C. Especel, P. Marécot, C.T. Williams, J. Catal. 275 (2010) 202–210.
[5] R.M.D. Nunes, B.F. Machado, M.M. Pereira, M.J.S.M. Moreno, J.L. Faria, J. Mol. Catal. A: Chem. 333 (2010) 1–5.
[6] Y.L. Liao, W.X. Que, J. Alloys Compd. 505 (2010) 243–248.
[7] M.M. Yea, Z.L. Chen, W.S. Wang, J.M. Shen, J. Ma, J. Hazard. Mater. 184 (2010) 612–619.
[8] M.S. Rana, J. Ancheyta, P. Rayo, S.K. Maity, Catal. Today 98 (2004) 151–160.
[9] M.S. Rana, J. Ancheyta, P. Rayo, S.K. Maity, Catal. Today 109 (2005) 61–68.
[10] A. Palani, H.Y. Wu, C.C. Ting, S. Vetrivel, K. Shanmugapriya, A.S.T. Chiang, H.M. Kao, Micropor. Mesopor. Mater. 131 (2010) 385–392.
[11] T. Prozorov, J. Wang, A.D. Ebner, J.A. Ritter, J. Alloys Compd. 419 (2006) 162–171.
[12] J. Jiang, L. Li, J. Alloys Compd. 456 (2008) 220–223.
[13] S. Gurmen, A. Guven, B. Ebin, S. Stopić, B. Friedrich, J. Alloys Compd. 481 (2009) 600–604.
[14] Y. Liu, Y. Zhao, L. Yu, Z. Wu, J. Alloys Compd. 485 (2009) L1–L4.
[15] S. Gurmen, B. Ebin, S. Stopić, B. Friedrich, J. Alloys Compd. 480 (2009) 529–533.
[16] W. Lv, B. Liu, Q. Qiu, F. Wang, Z. Luo, P. Zhang, S. Wei, J. Alloys Compd. 479 (2009) 480–483.
[17] M.S. Niasari, G. Hosseinzadeh, F. Davar, J. Alloys Compd. 509 (2011) 134–140.
[18] K. Yang, J.M. Zhu, J.J. Zhu, S.S. Huang, X.H. Zhu, G.B. Ma, Mater. Lett. 57 (2003) 4639–4642.
[19] H. Arami, M. Mazloumi, R. Khalifehzadeh, S.K. Sadrnezhaad, Mater. Lett. 61 (2007) 4559–4561.
[20] E. Ohayon, A. Gedanken, Ultrason. Sonochem. 17 (2010) 173–178.
[21] M.M. Mdleleni, T. Hyeon, K.S. Suslick, J. Am. Chem. Soc. 120 (1998) 6189–6190.
[22] J.H. Bang, K.S. Suslick, J. Am. Chem. Soc. 129 (2007) 2242–2243.
[23] G. Wu, X. Tan, G. Li, C. Hu, J. Alloys Compd. 504 (2010) 371–376.
[24] A. Majhi, G. Pugazhenthi, A. Shukla, Ind. Eng. Chem. Res. 49 (2010) 4710–4719.
[25] A. Vargas, J.A. Montoya, C. Maldonado, I. Hernández–Pérez, D.R. Acosta, J. Morales, Micropor. Mesopor. Mater. 74 (2004) 1–10.
[26] M.M. Mohamed, W.A. Bayoumy, M. Khairy, M.A. Mousa, Micropor. Mesopor. Mater. 103 (2007) 174–183.
[27] A. Beitollahi, A. Hossein, H. Daie, L. Samie, M.M. Akbarnejad, J. Alloys Compd. 490 (2010) 311–317.
[28] G. Wang, Q. Mu, T. Chen, Y. Wang, J. Alloys Compd. 493 (2010) 202–207.
[29] S. Li, Q. Shen, J. Zong, H. Yang, J. Alloys Compd. 508 (2010) 99–105.
[30] S.M. Morris, J.A. Horton, M. Jaroniec, Micropor. Mesopor. Mater. 128 (2010) 180–186.
[31] J.R. Grzechowiak, I.W. Zielińska, K. Mrozińska, Catal. Today 119 (2007) 23–30.
[32] J.A. Muñoz–López, J.A. Toledo, J. Escobar, E. López–Salinas, Catal. Today 133–135 (2008) 113–119.
[33] A.J. Duan, R.L. Li, G.Y. Jiang, J.S. Gao, Z. Zhao, G.F. Wan, D.Q. Zhang, W.Q. Huang, K.H. Chung, Catal. Today 140 (2009) 187–191.
[34] J. Aguado, J.M. Escola, M.C. Castro, Micropor. Mesopor. Mater. 128 (2010) 48–55.
[35] P. Padmaja, K.G.K. Warrier, M. Padmanabhan, W. Wunderlich, J. Sol–Gel Sci. Technol. 52 (2009) 88–96.
[36] N. Wang, H. Li, H. He, L. Han, J. Alloys Compd. 501 (2010) L38–L41.
[37] Y. Wang, J. Wang, M. Shen, W. Wang, J. Alloys Compd. 467 (2009) 405–412.
[38] S.A.H. Tabrizi, E.T. Nassaj, H. Sarpoolaky, J. Alloys Compd. 456 (2008) 282–285.
[39] X.C. Jiang, T. Herricks, Y.N. Xia, Adv. Mater. 15 (2003) 1205–1209.
[40] H.M. Yang, M.Z. Liu, J. Ouyang, Appl. Clay Sci. 47 (2010) 438–443.
[41] Y.S. Jung, D.W. Kim, Y.S. Kim, E.K. Park, S.H. Baeck, J. Phys. Chem. Solids 69 (2008) 1464–1467.
[42] A.H. Suna, P.J. Guo, Z.X. Li, Y. Li, P. Cui, J. Alloys Compd. 481 (2009) 605–609.
[43] M. Kruk, M. Jaroniec, Chem. Mater. 13 (2001) 3169–3183.
[44] N. Bejenaru, C. Lancelot, P. Blanchard, C. Lamonier, L. Rouleau, E. Payen, F. Dumeignil, S. Royer, Chem. Mater. 21 (2009) 522–533.
[45] M.M. Yusuf, H. Imai, H. Hirashima, J. Sol–Gel Sci. Technol. 28 (2003) 97–104.